Current Opinion in Solid State and Materials Science 21 (2017) 299–311

Contents lists available at ScienceDirect

Current Opinion in Solid State and Materials Science

journal homepage: www.elsevier.com/locate/cossms

Physical metallurgy of concentrated solid solutions from low-entropy to high-entropy alloys

Chun-Yang Cheng [a], Ya-Chu Yang [a], Yi-Zhen Zhong [a], Yang-Yuan Chen [b], Tung Hsu [a], Jien-Wei Yeh [a,*]

[a] Department of Materials Science and Engineering, National Tsing Hua University, Hsinchu 30013, Taiwan, ROC
[b] Institute of Physics, Academia Sinica, Taipei, Taiwan, ROC

ARTICLE INFO

Article history:
Received 4 March 2017
Revised 12 September 2017
Accepted 25 September 2017
Available online 28 September 2017

Keywords:
High-entropy alloys
Concentrated solid solutions
Physical metallurgy
Physical properties
Sluggish diffusion
Severe lattice distortion

ABSTRACT

The alloy world could be divided into low-entropy (LEAs), medium-entropy (MEAs) and high-entropy alloys (HEAs) based on the configurational entropy at the random solution state. In HEAs, four core effects, i.e. high entropy, sluggish diffusion, severe lattice distortion and cocktail effects, are much more significant than low-entropy alloys in affecting phase transformation, microstructure and properties. In fact, the degree of the influence from these core effects more or less increases with increased mixing entropy. The trend is gradual from low-entropy alloys to high-entropy alloys. In this article, physical metallurgy of HEAs is discussed with the bridge connected to that of conventional alloys. As disordered and ordered solid solutions are the main constituent phases of alloys, the understanding of solid solutions is fundamental for the understanding of alloys. In addition, as dilute solid solutions have been well treated in current physical metallurgy, concentrated solid solutions from low-entropy to high-entropy alloys are focused in this article. Physical properties are especially emphasized besides mechanical properties.

1. Introduction

Physical metallurgy is a science focusing on the relationships between composition, processing, crystal structure and microstructure, and physical and mechanical properties [1,2]. It has been developed for over one hundred years and become mature in the last century [1]. However, it is noted that physical metallurgy is almost based on the observations on conventional alloys having one major element or major compound. Whether physical metallurgy could be equally applied to those alloys without a base element or compound is an issue needed to be clarified. If there are some deviations found in certain items, more research would be required to make suitable modifications on the theories or even build up new concepts.

2. Alloy definition of concentrated solid solutions

Because all the concentrated alloys are multi-component no matter two or 30 components, it would be better to define concentrated alloys with suitable physical meaning. For example, non-equiatomic $Fe_{0.3}Co_{0.7}$ and equi-atomic FeCoCrMoNiTiSi alloys are belonged to the huge category of multi-component concentrated alloys but have little correlation. Except mixing entropy, metallurgical factors such as atomic size difference, mixing enthalpy, electronegativity, and valence electron concentration of alloys in the random solution state have no relation with the number of components. On the other hand, mixing entropy per mole, ΔS_{mix}, at the random state is a thermodynamic parameter having the same trend with the number of components and the degree of equalization of the concentrations between components. As configurational entropy per mole, ΔS_{conf}, calculated from the following equation contributes the main portion of mixing entropy at the random solid solution state, ΔS_{conf} is often used to represent mixing entropy:

$$\Delta S_{conf} = -R\sum_{i=1}^{n} X_i \ln X_i \quad (1)$$

where n is the number of components in the solid solution, X_i is the mole fraction of ith component, and R is the gas constant, 8.314 J $mol^{-1}K^{-1}$.

$T\Delta Sconf$ can be regarded as the driving force for a system towards the solid solutions with the random mixing of components. Consider a ΔS_{conf} which is equal to R and the equilibrium is at 1273 K, then $T\Delta Sconf$ has a value of 10.58 kJ/mol (=1273 K × 8.314 J mol^{-1} K^{-1}) and might counterbalance the

* Corresponding author.
E-mail address: jwyeh@mx.nthu.edu.tw (J.-W. Yeh).

https://doi.org/10.1016/j.cossms.2017.09.002
1359-0286/

increase of mixing enthalpy ΔH_{mix} (from several to tens kJ/mol) due to ordering or segregation and thus enhance the stability of solid solutions. As a result, a ΔS_{conf} of R might enhance the stability of solid solutions. This is why the entropy definition has been given for alloy systems: high-entropy ($1.5R \leq \Delta S_{conf}$), medium-entropy ($1.0R \leq \Delta S_{conf} \leq 1.5R$) and low-entropy alloys ($\Delta S_{\mathrm{conf}} \leq 1.0R$) although the boundary line could be somewhat relaxed [3–7]. This categorization illustrates the physical meaning that the driving force for component mixing is higher for medium-entropy alloys and even higher for high-entropy alloys. Although mixing enthalpy could be increased with the increased strain energy due to lattice distortion and with the increased chemical energy due to some loss of stronger chemical bonding (compared to ordering or segregation state), the tendency of mixing between elements still plays an important role to enhance the formation of multi-element disordered solid solution and/or intermediate phases (solid solutions with the stoichiometric compound structure) [8–10]. Definitely, the actual equilibrium state depends on the competition of mixing free energy ΔG_{mix} ($\Delta G_{mix} = \Delta H_{mix} - T\Delta Smix$) between mixing enthalpy and mixing entropy among different possible states and is that with the lowest free energy of mixing. For example, Fig. 1 shows the schematic curves of mixing Gibbs free energy for the $AlCoCrFeMo_{0.5}Ni$ alloy at (a) 673 K, and (b) 1273 K [10]. The "solid solution" curve is for the random solid solution, B2 and σ for multi-element ordered solid solutions (with B2 and σ structures, respectively), and FCC for multi-element random solid solution (with FCC structure). At 673 K, B2 and σ phases coexist whereas at 1273 K B2, σ and FCC phases coexist. It should be mentioned that multi-element composition feature of each phase was verified by the TEM-EDS analyses. This reflects that high entropy effect enhances the substitution between compatible elements.

Because the configurational entropy in the random solid solution state could be related with composition, there is a corresponding definition for alloys based on composition: A high-entropy alloy is defined as having at least five major metallic elements, each having an atomic percentage between 5% and 35% [3–6]. That is, $n_{major} \geq 5$ and $5\ at.\% \leq X_i \leq 35\ at.\%$. In general, medium-entropy alloys are those with 3–4 major elements and low-entropy alloys are those with 1–2 major elements.

3. Roles of four core effects in physical metallurgy

3.1. Four core effects

Because of their importance in influencing microstructure and properties, four core effects of HEAs were proposed in 2006 [4]. They are high entropy effect for thermodynamics, sluggish diffusion effect for kinetics, severe lattice distortion effect for structure, and cocktail effect for properties. Fig. 2 shows how these four core effects influencing physical metallurgy of HEAs [9,10]. High entropy effect should be considered in the free energies of different states to determine the equilibrium structure and microstructure and the driving force towards the equilibrium state. Sluggish diffusion effect affects the nucleation and growth rates in phase transformation. Severe lattice distortion effect affects the mechanical properties such as strength, strain rate sensitivity and ductility, and physical properties such as electrical resistivity and magnetism, which thus influence all conventional relationships between each property, structure and microstructure. In addition, it affects the strain energy, mixing enthalpy, lattice potential energy, diffusion, and recovery tendency which are important factors in thermodynamics and kinetics. Cocktail effect is the overall effect on properties from composition, structure and microstructure. Besides the mixture rule based on composition, interaction between elements, distorted lattice and phase distribution give excess amount of each property. Surely, there are other factors such as stress, temperature, and strain rate in processing or field application affecting the crystal structure, microstructure and properties, but these four core effects still exist.

For MEAs, the core effects in HEAs are expected in general lesser in degree. Same argument could be applied to LEAs. Therefore, for high-entropy concentrated solid solutions (HECSS), medium-entropy ones (MECSS) and low-entropy ones (LECSS), physical metallurgy principles might be different from that of current physical metallurgy because of the influence of these core effects. It is noted that current physical metallurgy mostly treats the pure metals and dilute solid solution (DSS). It can be expected that when physical metallurgy from conventional alloys to MECSS and even to HECSS are built, the basic understanding of the alloy world

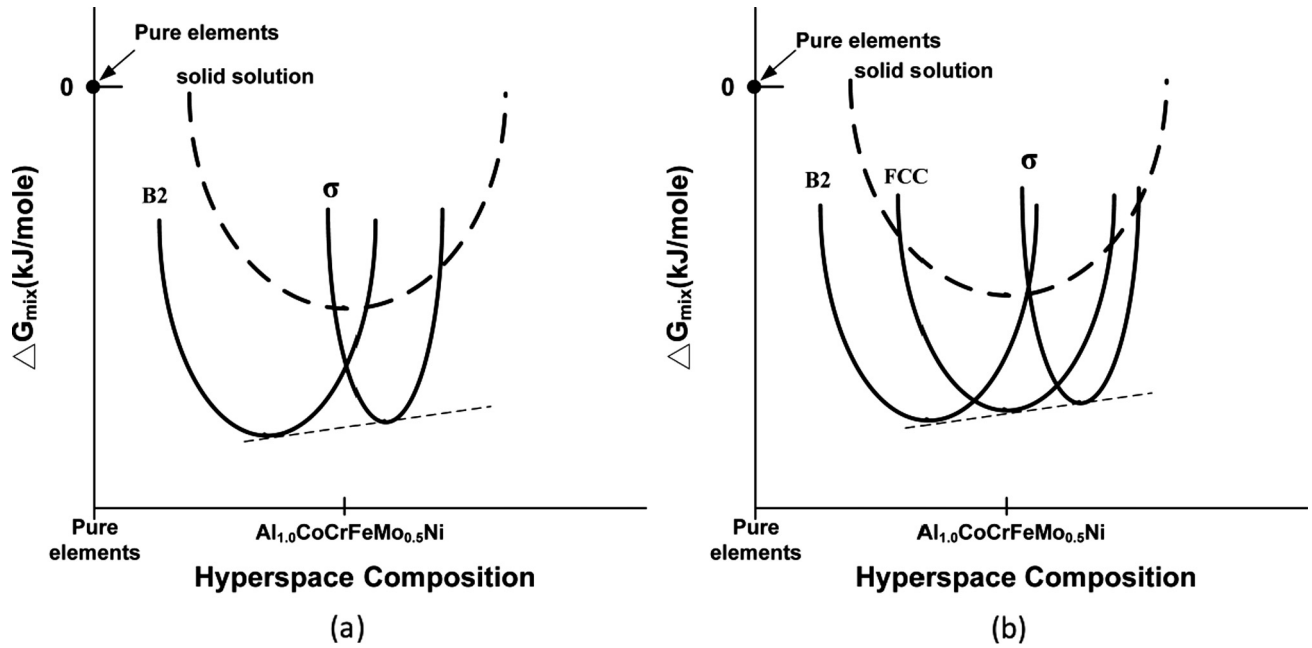

Fig. 1. Schematic curves of mixing Gibbs free energy for the $AlCoCrFeMo_{0.5}Ni$ alloy at (a) 673 K and (b) 1273 K [10].

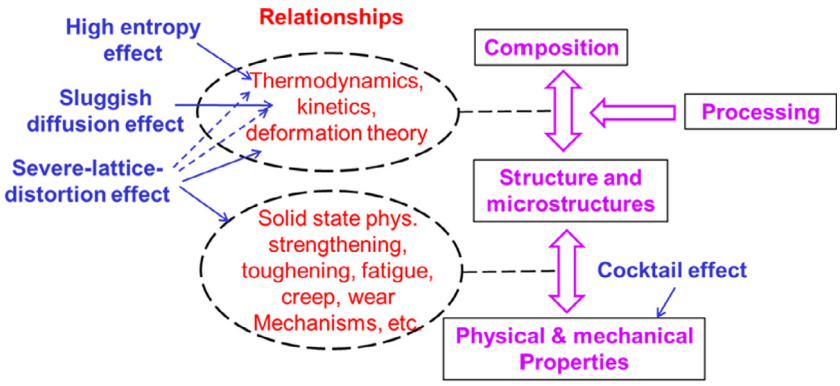

Fig. 2. The scheme of physical metallurgy and the influence from four core effects [9,10]. The solid arrows represent that the effect is direct and the dashed ones represent that the effect is indirect.

becomes realized. Besides forming single solid solution, HEAs might form two or more phases. They could be a mixture of stoichiometric compound, ordered concentrated solid solution (or intermediate phase), and disordered concentrated solid solution. Thus, the understanding of concentrated solid solutions is very helpful in understanding multi-phase HEAs.

3.2. Entropy effect in concentrated solid solutions

Entropy effect is often ignored in the phase prediction of conventional alloys. As a result, the equilibrium phase is often thought to be the outcome from the competition between the mixing enthalpies of competing phases. That means, the phases with the lowest overall mixing enthalpy would be the equilibrium phases based on the second law of thermodynamics. However, the mixing entropies of CSS phases are higher than that in conventional alloys. They should be considered in the prediction of their equilibrium phases. This is why the equilibrium phases at high temperatures are mainly multi-element disordered solid solutions and partially ordered multi-element solid solutions [6,9,10]. It is apparent that Hume-Rothery rules concern with the differences between two elements in terms of atomic size, crystal structure, valence electrons and electronegativity and entropy contribution is neglected [9,10]. However, as the prediction is for the high-temperature maximum solubility, the entropy contribution in concentrated binary alloy could not be neglected. From a qualitative base, the mixing entropy term (approximately configurational entropy) is the same for all binary alloys. The neglect is thought to be convenient. Now, when we considered the mixing entropy effect unary to high-order CSS, it should not be neglected as the effect is more and more important. That means, the mixing free energies of dilute solid solutions, concentrated solutions and intermetallic compounds need to compete with each other to determine the equilibrium state. Mixing entropy of high-order CSS becomes an important factor to stabilize their existence. It could counterbalance the strain energy of chemical energy increase due to lattice distortion energy and guarantee the stable existence of lattice-distorted CSS for potential studies.

3.3. Sluggish diffusion in concentrated solid solutions

In phase transformation theory, the formation of new phases from old phase requires cooperative diffusion of many different kinds of atoms to accomplish the partitioning of composition. The diffusion efficiency is expected to be lower than that in traditional alloys based on one major element. Thus, the nucleation and growth rates tend to be lower in HECSS. On the other hand, the diffusion of a species in HECSS would be slower due to lattice distortion which causes variations of lattice potential energy and higher activation energy along the diffusion path. The sluggish diffusion effect in HECSS thus includes both the lower diffusion rate of atoms and lower phase transformation rate in the whole solute matrix of a HECSS.

The first diffusion study on HEAs was made by using experimental alloys based on near-ideal FCC solid solution CoCrFeMnNi [11].The results were compared with that of three FCC pure metals (Fe, Co, and Ni), and four austenitic stainless steels containing higher concentration of Cr and Ni, as shown in Fig. 3. The diffusion coefficients of different atoms in the matrix have a general trend: Pure metal > MECSS > HECSS. On the other hand, melting-point-normalized activation energy shows the trend: HECSS > MECSS > Pure metal. This demonstrates the degree of sluggish diffusion effect could be expected to become more pronounced as more element and higher concentration are involved. That is, HECSS > MECSS > LECSS > DSS. The mechanism relates with lattice potential energy. Any atom in the lattice would experience fluctuated lattice potential energy due to different lattice distortion and coordination bonding along its diffusion path as shown in Fig. 4 and thus has higher activation energy to overcome deep traps [9,10].

3.4. Lattice distortion in concentrated solid solutions

In structure of HECSS, there is severe lattice distortion in the whole solute matrix since every atom on the lattice site has different first neighboring atoms and thus suffers lattice distortion due to atomic size difference, non-symmetric bonding and electron distribution [6,9,10]. As the degree of distortion depends on the difference in atomic size, chemical bonding and electron distribution transition among composing elements, more elements and high concentration in general cause severer distortion in CSS. Under this circumstance, crystalline imperfections (atomic-scale stress, strain, and energy levels around vacancy or atom, dislocation, stacking fault, grain boundary and twin boundary) on the distorted lattice of CSS would be quite different from DSS. . .and behaviors of imperfections on the lattice that influence deformation, and thus mechanical properties would be also quite different from those of pure metals. A discussion on this aspect from LECSS to HECSS based on Co-Cr-Fe-Mn-Ni has been made in Refs. [9,10] whereas further research and discussion are presented in the other articles of this special issue. On the other hand, diffuse scattering of X-ray beams, melting range, lattice constant, Young's modulus, thermal expansion, and electrical and thermal conductivities of a CSS and the theories on their correlations with lattice distortion are important and still lack at present. The main content in this study is thus intended to compare and bridge the basic properties between

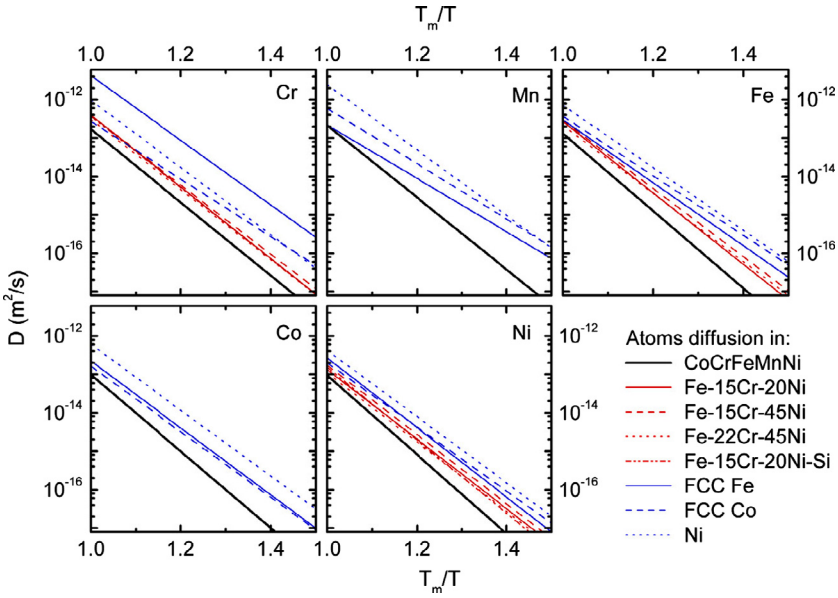

Fig. 3. Temperature dependence of the diffusion coefficients for Cr, Mn, Fe, Co, and Ni in different matrices: three pure metals, four MECSS and one HECSS [11].

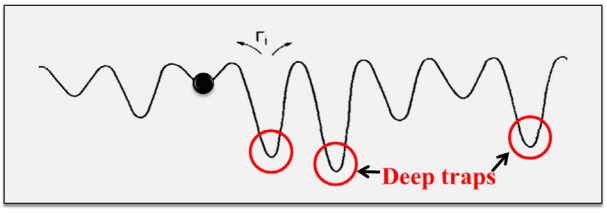

Fig. 4. Schematic diagram shows the fluctuation of lattice potential energy along the diffusion path for an atom in the lattice. Deep traps are indicated [9,10].

LECSS and HECSS in order to get full understanding. A series of Ni-Co-Fe-Cr-Mn alloys with single FCC structure for comparison on the same basis: Ni (pure metal), NiCo (LECSS), NiCoFe (MECSS), NiCoFeCr (MECSS), and CoCrFeMnNi (HECSS) were thus designed and investigated on crystal structure, X-ray diffraction intensity, local atomic configuration of lattice distortion, melting point, and thermal conductivity. The evolutions of lattice distortion effect was unveiled and then discussed with their mechanisms.

3.4.1. Experimental procedures for the series of Ni-Co-Fe-Cr-Mn alloys

Elemental Ni, Co, Cr, Fe, and Mn raw materials with purity levels exceeding 99.5 wt% were used to fabricate alloys. Their basic features and properties are given in Table 1 [12–15]. In the table, the lattice constants is of FCC structure, in which that of non-FCC Cr and Mn, although not found directly in the literature, have been calculated using the equation: $d_{FCC} = 4r_i/\sqrt{2}$, where r_i is atomic radius of element i in 12-coordinated metals [14,15].

All samples cut from rectangular ingots (40 mm × 10 mm × 20 mm) prepared via vacuum arc melting were encapsulated in quartz tubes under a vacuum of approximately 1×10^{-3} torr and then were homogenized at 1100 °C for 8 h with subsequent furnace cooling. After homogenization, the microstructures characterized by scanning electron microscope (SEM, JEOL JSM-5410) are uniform without any second phase (not shown in present work) to secure further analyses on same basis. The chemical composition is analyzed by SEM energy dispersive spectrometry (EDS). The crystal structure of the various alloys was identified using X-ray diffraction (XRD) (Rigaku ME510-FM2 diffractometer with Cu Kα radiation) at a scanning rate of 4°/min, a voltage of 30 kV, and a current of 20 mA. The scanning range was from 20 to 100°. High-temperature crystal structure and phase transition analysis were performed using a high-temperature X-ray diffractometer (HTXRD, SHIMADZU Lab XRD-6000) equipped with a vacuum heating stage (Anton Parr HTK 1200N). The working conditions are the same as described above. A turbo pump was used to maintain a vacuum of approximately 1.5×10^{-4} torr throughout the period of measurement. XRD patterns were recorded at 25, 100, 200, 300, 400, 500, 600, 700 and 800 °C. The heating rate from one temperature to the next was 50 °C/min and the holding time before diffraction at each tested temperature was 15 min. It should be mentioned that HTXRD samples were prepared by rasping the as-homogenized alloys into powders, and compressing the powder into the sample holder to produce a layer 0.4 mm in thickness. To eliminate residual stress in the particles, the holder with compacted powder was annealed in a vacuum chamber of HTXRD under 1×10^{-3} torr at 600 °C for 30 min and in-situ cooled. The HTXRD was then performed by heating again to each testing

Table 1
Properties of constituent elements in Ni-Co-Fe-Cr-Mn alloy series [12–15].

Element	Ni	Co	Fe	Cr	Mn
Crystal structure (20 °C)	FCC	HCP	BCC	BCC	SC
Atomic radius (Å)	1.25	1.25	1.27	1.28	1.26
Lattice constant (Å)	3.524	3.544	3.555	3.620	3.564
Melting point (°C)	1455	1495	1538	1863	1244
Specific heat (J g^{-1} K^{-1})	0.444.	0.421	0.449	0.449	0.479
Thermal conductivity (W m^{-1} K^{-1})	90.7	100	80.2	93.7	7.82

temperature in sequence. Densities were determined using the Archimedes method. Thermal diffusivity was measured using a laser flash device (NETZSCH model LFA 457 Microflash). The samples were in disk form with a diameter of 10 mm and a thickness of 3 mm. All samples were measured at temperatures between 25 °C and 400 °C. The local atomic configuration was investigated by using the extended X-ray absorption fine structure (EXAFS) technique with titanium K-edge core at the Wiggle-C Beamline BL17C of the National Synchrotron Radiation Research Center (NSRRC) in Hsinchu, Taiwan. EXAFS data were collected from thin foil of pure Ni and homogenized NiCoFeCrMn alloy. The data belong to pure Ni foil were collected in the transmission mode and used as empirical standards of the FCC structure. For NiCoFeCrMn the extended fine structure appearing from 30 to 950 eV above the absorption edge were isolated and normalized to the edge step height and energy, thus putting all data on a per atom basis. Residual, nonoscillatory curvature in the data was eliminated by fitting and removing a cubic spline curve using three equidistant internal knots. These data were Fourier transformed to radial coordinates (**R**).

3.4.2. X-ray diffraction analyses and lattice constant variation

Fig. 5 presents the HTXRD patterns of as-homogenized specimens from 25 to 800 °C. It reveals that each specimen is a single face-centered cubic (FCC) solid solution phase. Fig. 6 shows the room temperature (25 °C) XRD patterns of as-homogenized Ni to NiCoCrFeMn alloys extracted from Fig. 5. Slight peak shift owing to the variation of lattice constant is obvious (see brown dot line in Fig. 6). The corresponding experimental lattice constants (d_{exp}) which were obtained by extrapolation to $\theta = 90°$ for eliminating systematic errors are listed in Table 2. The $d_{avg,EDS}$ and d_{avg} in the 3rd and 4th columns of Table 2 are calculated based on EDS analyses and the rule of mixture (Vegard's law [16]), respectively. Results of EDS analyses corresponding to $d_{avg,EDS}$ of Ni-Co-Fe-Cr-Mn alloy series are also listed in Table 3, pointing out the chemical compositions are in agreement with equiatomic design concept.

Values of $d_{avg,EDS}$ are in accordance with those obtained by Vegard's law. However, d_{exp} values of Ni-Co-Fe-Cr-Mn alloy series except for NiCo present increasingly positive deviations from those predicted by EDS and the rule of mixture. The increased percentage of d_{exp} for NiCoFeCrMn is up to 1.4%. Bozzolo et al. stated that overall formation enthalpy for binary alloy systems, which would bring about the variation of lattice constant, is a competition of chemical bonding energy, i.e. mixing enthalpy, and strain energy caused by lattice distortion [17]. They have demonstrated that the lattice constant contraction of Au-Ag system is due to an attractive chemical bonding energy dominating a weak strain energy induced by small lattice mismatch [17]. Since the mixing enthalpy is increased slightly with the number of components listed in Table 4 [18,19] and would result in a small decrease of lattice constant due to shorter bond length [17], the actual increase of lattice constants gives a strong suggestion that lattice distortion, which is shown in Fig. 8 from the analysis of the local atomic configuration using EXAFS technique, has the effect to expand the lattice.

The mechanism of local atomic variation inducing lattice distortion and expansion is proposed for this phenomenon in this study. In a pure metal under equilibrium condition, all atoms occupy their normal lattice sites with symmetrical interatomic force balances. The atomic packing would be at the most compact condition and have a minimum atomic volume. If we displace an atom to have an offset from its normal lattice site, the displacement would locally disturb the symmetrical binding and balance between atoms and cause local volume to expand slightly. If more atoms are displaced from their normal sites, the average atomic volume would increase correspondingly. Consequently, a distorted lattice with zigzag atomic directions and planes would disturb the original lattice to have a certain expansion of volume. For an ideal solid solution in which no excess atomic bonding exists, the actual lattice distortion would result in larger experimental lattice constant, d_{exp}, than d_{avg}, as d_{avg} is the lattice constant of an average structure which is simply the average of the equilibrium structure of component elements without taking lattice distortion into account. In reality, atomic size difference would adjust the atoms from their ideal position to new positions for strain release and energy release. This adjustment would in turn reduce the bonding energy, and increase bond length and lattice constant. Moreover, Lubarda's approach defining the unit cell of a binary alloy have been extended to multi-principal component alloys to calculate lattice constant in HEA by Toda-Caraballo et al., in which atomic size mismatch is considered [20,21]. The lattice constant of NiCoFeCrMn calculated by this approach is larger than that of NiCoFeCr. This result is consistent with expansion effect observed in the present study. Therefore, in the present alloy series, this expansion effect by lattice distortion is clearly revealed: the excess atomic bonding, i.e. negative ΔH_{mix} in Table 4, in reducing lattice constant is still small to counterbalance the expansion from atomic size difference.

3.4.3. Atomic configuration and origin of lattice distortion obtained by EXAFS analyses

X-ray absorption spectroscopy (XAS) measures the absorption of x-rays as a function of X-ray energy for a material. It is also referred to as X-ray Absorption Fine-Structure (XAFS) which is the modulation of the X-ray absorption coefficient at energies near and above an X-ray absorption edge and can be broken into 2 regimes: X-ray-absorption near-edge structure (XANES) and extended X-ray absorption fine-structure (EXAFS) [22]. Here we only interested in EXAFS. EXAFS is a region of XAFS which is started approximately from 30 eV above the absorption edge and contains information about the local atomic structure around the atom absorbed the X-ray [23]. Fig. 7 shows the Fourier transforms of the EXAFS K-edge spectra for each element in NiCoFeCrMn alloy, in company with standard FCC-Ni spectra for comparison. Compared the peak positions of all elements with typical peak positions of pure Ni, the local atomic configuration of all elements in the NiCoFeCrMn alloy is also of FCC. This clearly demonstrates that all component atoms mutually mix in the FCC lattice and form an FCC solid solution. This is consistent with the single FCC phase observed in the XRD pattern of NiCoFeCrMn alloy. The first peak (R_1) in Fig. 7 corresponds to the first neighboring shell in FCC structure and the subsequent peaks correspond to shells of the second (R_2), third (R_3), and so on. The R_1 value of pure FCC Ni is 2.148 Å lower than the expected value (2.492 Å) in the framework of the hard balls description due to uncorrected electron phase shifts [24,25]. Moreover, the R_1 value of Ni in NiCoFeCrMn alloy (2.178 Å) is greater than that of pure Ni (2.148 Å). This positive shift suggests the nearest-neighbor bond is greater in the NiCoFeCeMn alloy than in the pure FCC Ni standard, a result in accordance with the larger lattice constant measured in NiCoFeCrMn alloy using X-ray diffraction (Table 2). Such result is attributed to change in surrounded atoms for Ni when Ni equiatomically alloyed with Co, Fe, Cr and Mn and similar to the outcomes obtained by Harris et al. [25]. Because Ni has the strongest tendency to stabilize FCC structure and occupies the exact lattice site and Ni spectrum in NiCoFeCrMn alloy is almost same as that of pure Ni regardless of slight peak location shift, Ni-position could be regarded as a reference when comparing the relative peak positions of Co, Fe, Cr, and Mn to those of Ni. This comparison could give information of the deviation of component atoms from Ni-position. Table 5 shows the three peak positions of R_1, R_3 and R_4 for Ni, Co, Fe, Cr, and Mn in NiCoFeCrMn alloy and the deviation from Ni-position for comparison. R_2 is not compared because of its small peak and poorer resolution. It is noted that only Co has positive deviation (+1.4%) from Ni-position at R_1 indicating its strong tendency to

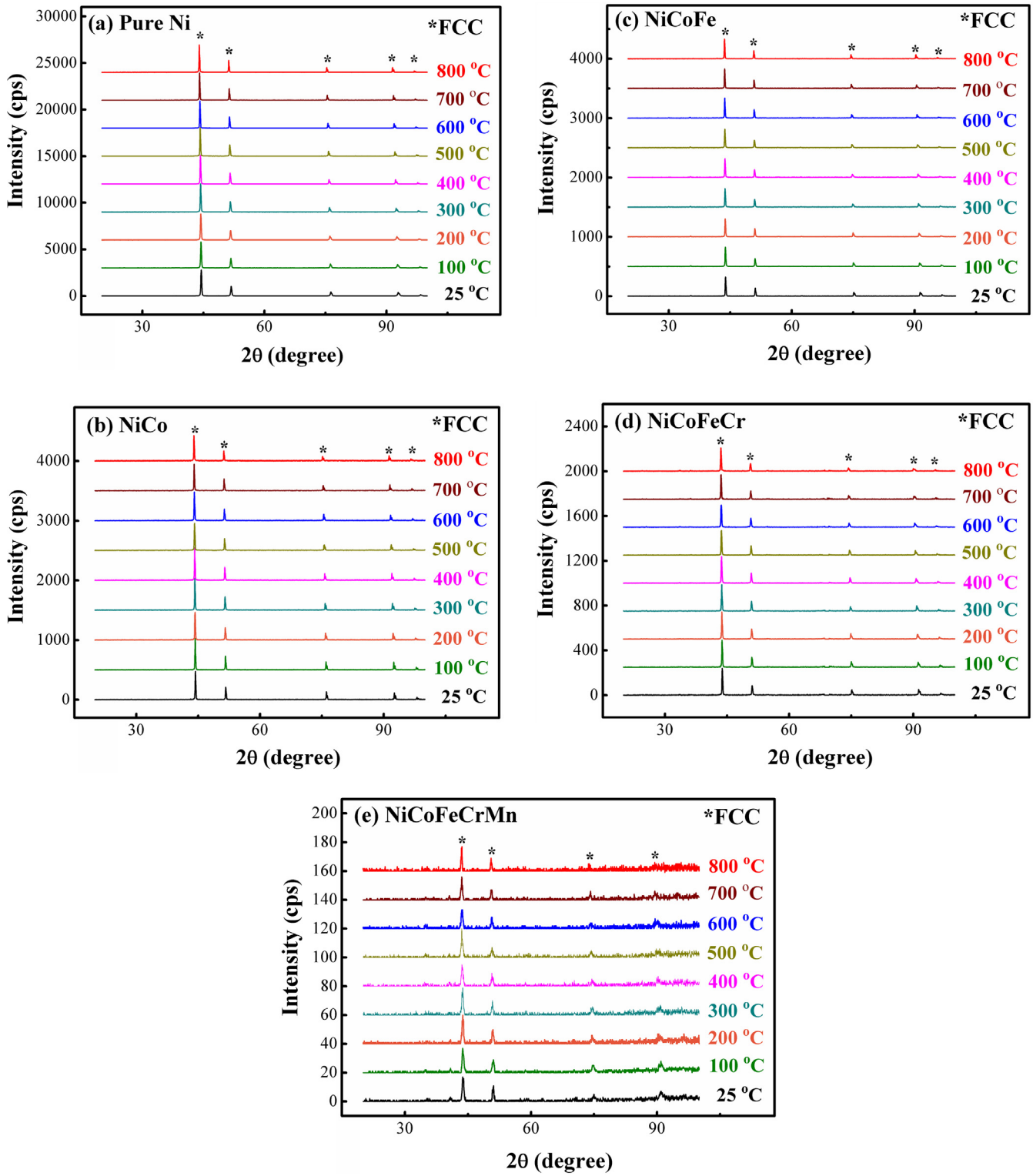

Fig. 5. XRD diffraction patterns from 25 to 800 °C for as-homogenized (a) Ni, (b) NiCo, (c) NiCoFe, (d) NiCoFeCr, and (e) NiCoFeCrMn.

shift from exact lattice site. Co, Fe, and Cr have similar negative deviations (−0.8%), but Mn has positive deviation (+0.8%) from Ni-position at R_3. Furthermore, Co and Cr show negative deviation (−0.7%), Mn do nothing, and Fe do positive deviation (+0.7%) from Ni-position at R_4. These positive and negative deviations illustrate that the lattice of NiCoFeCrMn alloy is distorted at every lattice site since each kind of atom has some offset from the lattice sites. Among them, Co has the largest deviation or distortion. Mn has the lowest deviation.

Peak shapes for individual element are different as well. The shape of a peak indicates the spatial distribution of atoms across its shell circle. It can be seen that the local spectrum shapes at R_3 and R_4 of Fe are similar to that of Ni, but those of Co, Cr, and Mn differ a lot from that of Ni in the NiCoFeCrMn alloy. Co has sharp

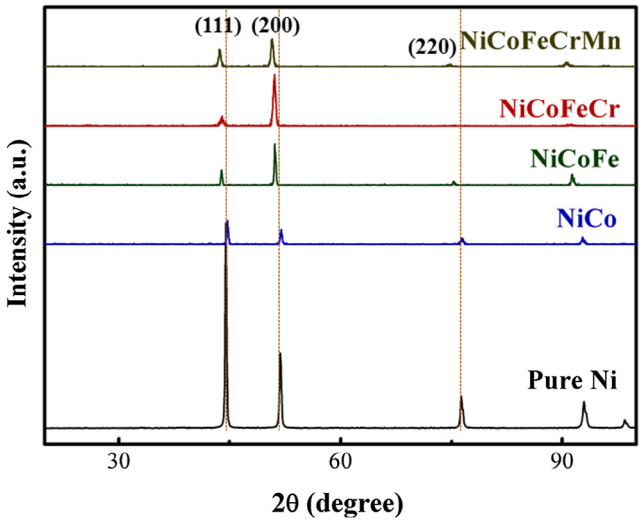

Fig. 6. Room temperature (25 °C) XRD analyses of: (a) Ni, (b) NiCo, (c) NiCoFe, (d) NiCoFeCr, and (e) NiCoFeCrMn under as-homogenized conditions. The brown dot lines are used to mark the peak positions of Ni.

Table 2
Experimental lattice constants (d_{exp}) and the average lattice constants obtained by EDS analysis ($d_{avg,EDS}$) and rule of mixture (d_{avg}).

Alloy	d_{exp} (Å)	$d_{avg,EDS}$ (Å)	d_{avg} (Å)
NiCo	3.532	3.534	3.534
NiCoFe	3.569	3.541	3.541
NiCoFeCr	3.589	3.562	3.561
NiCoFeCrMn	3.612	3.561	3.561

Table 3
Large-area EDS analyses of as-homogenized specimens of NiCo, NiCoFe, NiCoFeCr, and NiCoFeCrMn, respectively.

Alloy	Content of constituent element (at.%)				
	Ni	Co	Fe	Cr	Mn
NiCo	50.2	49.8	–	–	–
NiCoFe	33.0	33.6	33.4	–	–
NiCoFeCr	24.4	24.9	24.7	26.0	–
NiCoFeCrMn	20.2	19.3	20.9	20.2	19.4

Table 4
Mixing enthalpy (ΔH_{mix}), atomic size difference (δ), and melting point $T_{m,rom}$ of the experimental alloys [18,19].

Alloy	ΔH_{mix} (kJ/mol)	δ	$T_{m,rom}$
NiCo	0	0	1474
NiCoFe	−1.33	0.75	1495.3
NiCoFeCr	−3.75	1.06	1590.3
NiCoFeCrMn	−4.16	0.92	1521

peaks at R_2, R_3 and R_4 whereas those of Ni and Fe have some overlapping between R_2 and R_3, and between R_3 and R_4. On the other hand, Cr and Mn have more overlapping between R_3 and R_4 than Ni and Fe. This suggests that spatial distributions of Co at the second, third, and fourth shells are narrower than those of Ni and Fe whereas those of Cr and Mn are broader. Overlapping of EXAFS peaks stems from the amplitude contribution of neighbor atoms as well as a photoelectron focusing effect caused by the collinear arrangement of the lattice sites [25]. Moreover, the deviation of peak position for Co, Fe, Cr and Mn from Ni could affect the collinear arrangement of the lattice sites, further leading to alteration

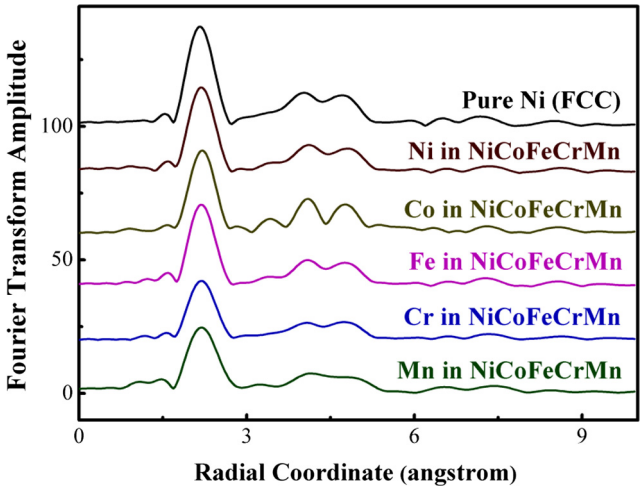

Fig. 7. Fourier transforms of the EXAFS K-edge spectra of Ni, Co, Fe, Cr, and Mn in NiCoFeCrMn alloy. That of pure Ni is compared.

of overlapping. As a consequence, here we interpret that deviation of peak position together with difference of spatial distribution of atoms in NiCoFeCrMn alloy is attributed to atomic size, crystal structure in its pure metal form, and chemical bonding differences. Crystal structure difference is the difference of crystal structures between pure elements such as Ni and Co which are FCC and HCP, respectively. Chemical bonding difference mainly comes from the difference of electronic and magnetic interactions between atomic pairs connected to the same lattice point. For example, Co-Fe, Co-Mn, Co-Cr, and Co-Co chemical bond strength and orientation around a Co atom are different and cause unsymmetrical interatomic forces on the Co atom. All these factors would be responsible for lattice distortion. Different elements have different reasons to cause lattice distortion. For example, as the atomic size, electronegativity, and valence of Co are close to that of Ni (see Table 1) and also small ΔH_{mix} (this reflects their similarity in electronegativity and valence) between Ni and Co, the deviation of Co from Ni position is mainly attributable to the crystal structure difference. In contrast, reasons for peak deviations (R_1, R_3 and R_4) of Fe, Cr and Mn would be the combined effect of appreciable atomic size, crystal structure, and chemical bonding differences. But how their individual effects on R_1 position are additive or subtractive and how their mutual interference and final compromise among different atoms still need further study. The distortion phenomena have also been identified by using EXAFS technique for $Au_{1-x}Ni_x$ solid solution [26] and ordered and disordered Cu_3Pd alloys [27]. In the former, the positive deviation of the lattice parameter from Vegard's law introduced by lattice distortion was found. It was also concluded that although the solid solutions are crystalline, the atoms are strongly displaced with respect to their regular location in an undistorted lattice. In the latter, it was concluded that a distribution of bond length must exist in the random alloy in order for the distorted first shell of neighbors to be accommodated.

3.4.4. Lattice distortion effect on XRD peak intensity

Both temperature and lattice distortion have significant effects on XRD intensity. An increase in temperature causes vibrating atoms to deviate from their neutral positions resulting in a roughening of diffraction planes and thus lowers the intensity of reflected X-rays. This temperature effect has been described using the Debye-Waller temperature factor (M^T) [15,28,29] as follows:

$$M^T = 8\pi^2(\bar{u}^2)^T\left(\frac{\sin\theta}{\lambda}\right)^2 = \frac{6h^2T}{mk\Theta^2}\left(\phi(x)+\frac{x}{4}\right)\left(\frac{\sin\theta}{\lambda}\right)^2 \quad (2)$$

Table 5
Peak positions of R_1, R_3 and R_4 for Ni, Co, Fe, Cr, and Mn in NiCoFeCrMn alloy, and their deviations from Ni-position in percentage.

Element	Ni	Co	Fe	Cr	Mn
R_1 (Å)	2.178	2.209 (+1.4%)	2.178 (0%)	2.178 (0%)	2.178 (0%)
R_3 (Å)	4.111	4.080 (−0.8%)	4.080 (−0.8%)	4.080 (−0.8%)	4.142 (+0.8%)
R_4 (Å)	4.786	4.755 (−0.7%)	4.817 (+0.7%)	4.755 (−0.7%)	4.786 (0%)

where $\overline{u}^T$ is the amplitude of the vibrations in the atoms; θ and λ are the angle and wavelength of the incident X-ray beam, respectively; h is the Planck constant; T is the absolute temperature; m is the mass of the vibrating atoms; k is the Boltzmann constant; Θ is the Debye characteristic temperature of the substance, $x = \Theta/T$; and $\varphi(x)$ is the function associated with values of Θ.

Correlating M^T with the structure factor F_{hkl} on the (hkl) crystal plane originally at absolute temperature 0 K enables the expression for the structure factor at different temperature, $\overline{F}^T_{hkl} = F_{hkl}\exp(-M^T)$. On the other hand, lattice strains or distortions in the atomic planes caused by residual stress or applied plastic deformation have been shown to cause a shift in the peak or a decrease in intensity with peak broadening in the diffraction lines [15,28,29].

According to a previous study on high-entropy alloys, differences in atomic size among composing elements would lead to a severe lattice distortion which further reduces the peak intensities in XRD patterns [30]. This effect was proposed to be similar to the effect of temperature on XRD intensity and can be formulated using another modification factor, referred to as the lattice distortion factor (M^D) [30],

$$M^D = 8\pi^2(\overline{u}^2)^D\left(\frac{\sin\theta}{\lambda}\right)^2 \quad (3)$$

where $\overline{u}^D$ is the deviation displacement of atoms caused by intrinsic lattice distortion. However, according to the present analyses of EXAFS in last section, the lattice distortion previously attributable to atomic size difference should include the effect from crystal structure difference and bonding strength difference. Final compromise among different atoms to lower the total free energy would be also a factor.

In Fig. 5, X-ray diffraction peak intensities in terms of counts per second (cps) show the typical decrease in height with increasing number of component in Ni-Co-Fe-Cr-Mn alloy series. Furthermore, we compare integrated intensities of (1 1 1) plane at 25 and 800 °C as a function of the number of components in the alloy series illustrated in Fig. 8. From Fig. 8 although integrated intensity significantly decreases from Ni to NiCoFeCrMn at 25 and 800 °C, the peak intensity of Ni to NiCoFeCrMn is not sensitive to temperature from 25 to 800 °C.

In order to clarify the intrinsic effect of temperature and lattice distortion on XRD intensity, HTXRD investigation was also conducted on two FCC pure metals, aluminum and silver, as shown in Fig. 9. It can be seen from Fig. 9(b) and (d) that the (1 1 1) integrated XRD intensities of Al and Ag did not drop from room temperature level until 300 °C ($0.61T_{m,Al}$) and 400 °C ($0.55T_{m,Ag}$), respectively,. These two metals tell us that 0.55 T_m could be regarded as the least temperature for the significant decrease of peak intensity. This is reasonable in view of the fact that thermal vibration amplitude becomes large to begin the effective thermal activation at around recrystallization temperature 0.5 T_m, which would also turn on the effective diffuse scattering. Now, consider (1 1 1) integrated intensity of pure Ni, respectively, at room temperature and 800 °C. Since 800 °C is equal to $0.62T_m$ which is higher than $0.55T_m$, the intensity at 800 °C is expected to be lower than that at room temperature. This agrees well with the present observation. We can see a 22% decrease from room temperature to 800 °C for pure Ni (Fig. 8). Further check on NiCo, NiCoFe, NiCoFeCr and NiCoFeCrMn alloys, a similar decrease is also seen despite their integrated intensities are low (the actual values of integrated intensity of NiCoFeCrMn at 25 °C and 800 °C are 17 and 13 cps). This is expected since their temperature factors (M^T) in Eq. (2) are similar at the same temperature of 800 °C although there might be some difference in m and Θ.

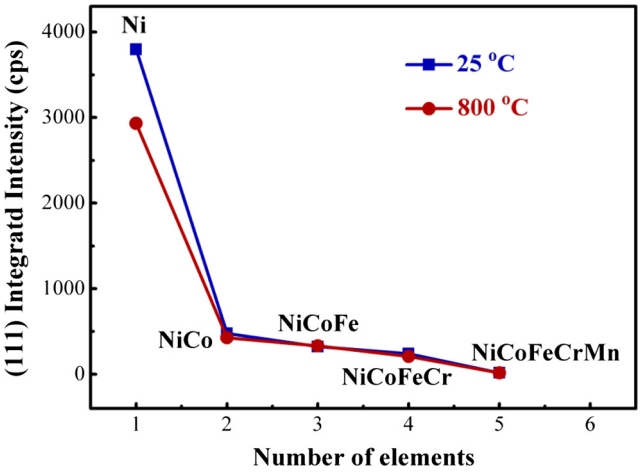

Fig. 8. Evolution of (1 1 1) integrated XRD intensity in the as-homogenized Ni-Co-Fe-Cr-Mn series.

In contrast, remarkable diffuse scattering effect of lattice distortion due to multi-element effect on intensity is seen at 25 and 800 °C. The intensity has a large drop from Ni to NiCo and continues to decrease as the number of component increases. This suggests that Co has a large diffuse scattering effect. In fact, this effect is consistent with the observation from EXAFS analyses. Co has positive deviation (+1.4%) from Ni-position at R_1, and negative deviations, −0.8% and −0.7%, at R_3 and R_4, respectively. In addition, Co has a narrower distribution at second, third and fourth shells than Ni. Therefore, combination of these two factors, i.e. non-regular position and distribution, yields significant lattice distortion which in turn brings large overall effect on diffuse scattering as compared with Fe, Cr, and Mn (see Eq. (3)). This phenomenon echoes the conclusion in last section that not only atomic size difference among composing elements but also their crystal structure difference and the bonding strength difference due to interatomic interaction could have the effect on lattice distortion. Because lattice distortion due to different features of dissimilar components is little affected by temperature, its remarkable diffuse scattering is expected to be similar even at 0 K. Therefore, such lattice distortion far exceeds the lattice distortion contributed by thermal vibration from 0 K to 1073 K (or 800 °C) in the present alloy series. It should to be mentioned that the mechanism of diffuse scattering, i.e., interaction between X-ray beam with electrons and atoms, might

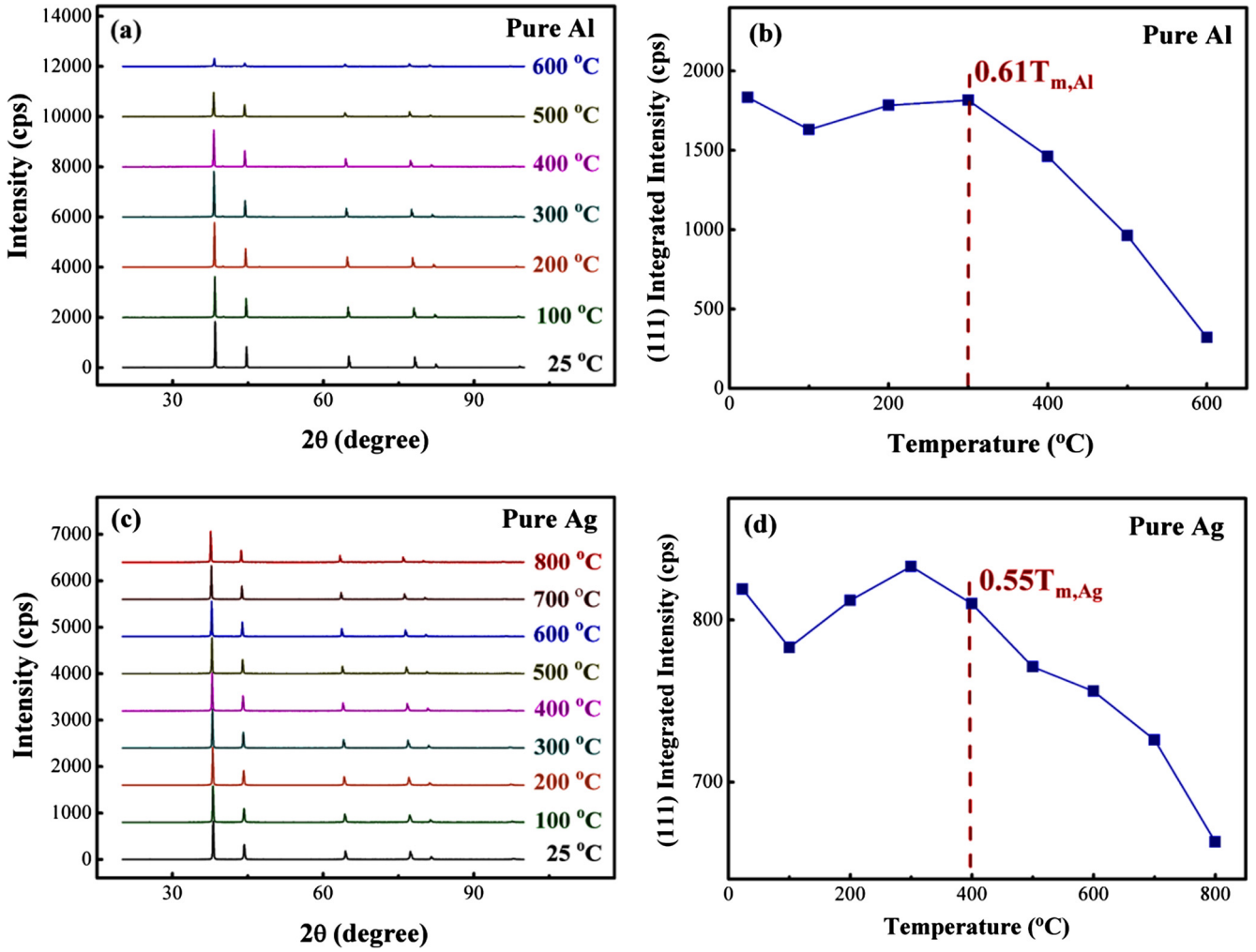

Fig. 9. HTXRD spectra of (a) pure Al and (c) pure Ag from 25 to 800 °C, and (1 1 1) integrated intensity of (b) pure Al and (d) Ag.

be different from other mechanisms. For example, a large diffusion scattering of NiCo doesn't lead to large solution hardening in plastic deformation although both are affected by lattice distortion. The solution hardening theoretically relates atomic size difference, Young's modulus difference, ordering and so on. The small hardness increases from HV72.6 of Ni to HV79.3 of NiCo is apparently consistent with their similarity in atomic size and bonding. In brief, different mechanisms emphasize different points of lattice distortion, which requires further investigations in the future.

3.4.5. Lattice distortion effect on melting point

Lattice distortion could have another effect in lowering the melting point predicted by the rule of mixture for this alloy series. Fig. 10 shows solidus temperature (T_s) and liquidus temperature (T_l) of as-homogenized Ni-Co-Fe-Cr-Mn alloy series measured by differential scanning calorimetry (DSC, curves not shown). The melting range for NiCo, NiCoFe, NiCoFeCr, and NiCoFeCrMn are 30, 30, 25, and 50 °C, respectively. In order to find the reason of temperature drop in Fig. 10, we compare average melting temperature ($T_{m,avg} = (T_s + T_l)/2$) with that, $T_{m,rom}$, calculated by the rule of mixture, $T_m = \sum X_i T_m^i$, where X_i and T_m^i are the molar fraction and melting temperature of constituent element i, respectively [18]. Consider $T_{m,avg}$ and $T_{m,rom}$ of binary NiCo, no difference between $T_{m,avg}$ and $T_{m,rom}$ is seen. This result represents that its melting temperature can be perfectly predicted by the rule of mixture. Nonetheless, changes in the melting temperature of other alloys

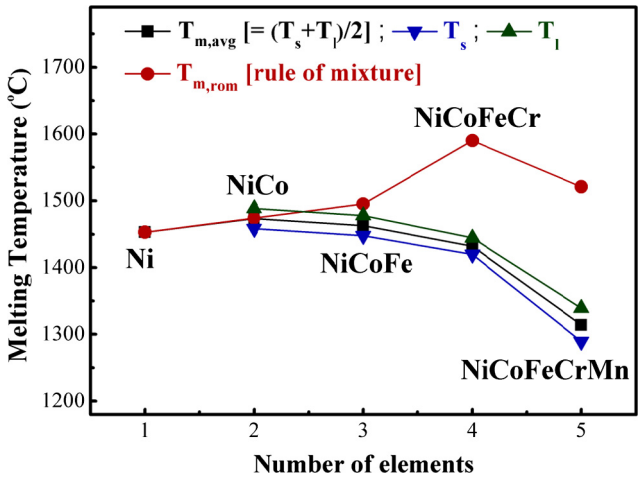

Fig. 10. Developments of melting temperatures under various definitions of as-homogenized Ni-Co-Fe-Cr-Mn alloy series.

in the Ni-Co-Fe-Cr-Mn system cannot be predicted perfectly using the rule of mixture.

As shown in Fig. 10, T_s, T_l, and $T_{m,avg}$ decrease with an increase in the number of incorporated elements from binary to quinary alloy. However, the trend of $T_{m,rom}$ changing with the number of

elements is quite different. $T_{m,rom}$ increases to a maximum at NiCoCrFe and then decreases when Mn is added. The discrepancy between $T_{m,rom}$ and $T_{m,avg}$ requires further discussion. Oates considered the effect of configurational entropy on the stabilization of liquid phase for a simple eutectic system (the liquid phase is ideal and the two pure solids, of identical melting points and entropies of fusion, are completely immiscible) [31]. He concluded from thermodynamic calculation that the liquid is stabilized by configurational entropy since the solid without any mutual solubility has no configurational entropy. The eutectic point is lower than that of the arithmetic average of the two components. In addition, the extent of the phase stability domain for the liquid phase is determined by the magnitude of the configurational entropy of mixing in similar multicomponent system. Ten-component alloys would show much larger liquid domain and lower eutectic points than binary alloys. Although this hypothetical system is an extreme case, it indicates that configurational entropy has the effect to lower the melting point or melting range predicted by the rule of mixture if the alloys at the solid state are not completely miscible and thus have smaller configurational entropy than their liquid state.

Besides the configurational entropy effect, lattice distortion in the solid state as well as chemical bonding energy change from solid to liquid might also affect melting point, which can be calculated and explained by thermodynamics. If an alloy system in which components are completely miscible in the solid state, the configurational entropy is nearly the same between solid and liquid. Thus, configuration entropy would have little effect on the melting point. However, mixing enthalpy contributed by chemical bonding difference between solid and liquid states and the strain energy due to lattice distortion (strain energy is zero in the liquid state) becomes the main factor. It is well known from thermodynamics that positive mixing enthalpy would cause liquidus line to show a minimum, and conversely negative mixing enthalpy would cause it to show a maximum. This is because the liquid state has a larger interatomic distance and thus weaker interatomic interaction than the solid state [32,33]. For the sake of simplicity in the calculation, consider a hypothetical binary system in which A and B components have the same melting point and form regular solid solution with mixing enthalpy partly from excess chemical bonding between A-B pair and partly from strain energy due to lattice distortion [17], then melting temperature drop due to these two contributions could be easily derived. Based on the mixture rule, the melting temperature of the hypothesized alloy is the same as that of both components. At the melting temperature, the change in Gibbs free energy per mole would be equal to zero for both components, and can be written as:

$$\Delta G_0^{s\to l} = \Delta H_0^{s\to l} - T_{m0}\Delta S_0^{s\to l} = 0, \quad \text{thus} \quad \Delta S_0^{s\to l} = \frac{\Delta H_0^{s\to l}}{T_{m0}} \tag{4}$$

where T_{m0} is the melting temperature, $\Delta H_0^{s\to l} > 0$ is the latent heat, and $\Delta S_0^{s\to l} = \frac{\Delta H_0^{s\to l}}{T_{m0}}$ is the entropy change during fusion. Now for any composition of the binary alloy, since the change in free energy during fusion is also zero and moreover the entropy change from solid configuration to liquid configuration is approximately the same as both components, i.e., $\Delta S_0^{s\to l} = \frac{\Delta H_0^{s\to l}}{T_{m0}}$, the free energy change per mole can be expressed as:

$$\Delta G_0^{s\to l} = \Delta H_1^{s\to l} - T_{m1}\Delta S_0^{s\to l} = 0 \tag{5}$$

where T_{m1} is the melting temperature of the alloy after mixing, and $\Delta H_1^{s\to l} > 0$ is the latent heat. Because the melting of the alloys is in a temperature range except the minimum or maximum point at certain composition, the melting temperature here is defined as the temperature at which the free energy of solid phase is equal to that of liquid phase, as expressed by Eq. (5). This is convenient because it is approximately equal to the average melting temperature ($T_{m,avg} = (T_s + T_l)/2$) mentioned above. Consequently, the latent heat becomes

$$\Delta H_1^{s\to l} = \Delta H_0^{s\to l} - \Delta H_{strain} - \Delta H_{chem} \tag{6}$$

where ΔH_{strain} and ΔH_{chem} are strain energy and chemical bonding energy difference between solid state and liquid state at this composition, respectively. Since the liquid state could release any strain energy by its fluid behavior, the strain energy ΔH_{strain} is exactly equal to the lattice-distortion strain energy in the solid. On the other hand, as stated in the above that the liquid state has a larger interatomic distance and weaker interatomic interaction than the solid state, the ΔH_{chem} is smaller in magnitude than that of solid state [32,33]. Substituting Eqs. (4) and (6) into (5), we obtain

$$\frac{T_{m0} - T_{m1}}{T_{m0}} = \frac{\Delta H_{strain} + \Delta H_{chem}}{\Delta H_0^{s\to l}} \tag{7}$$

As $\Delta H_0^{s\to l} > 0$, strain energy due to lattice distortion in the solid state and chemical bonding energy difference between solid state and liquid state clearly play a role in altering the melting temperature. The melting temperature drop or increase as compared with that based on the mixture rule thus depends on the difference between these two quantities. If ΔH_{chem} is zero, that means A and B components have no extra interaction, the strain energy due to lattice distortion would lower the melting temperature and larger strain energy would give a larger drop. If the strain energy is zero, negative ΔH_{chem} would cause a temperature increase and vice versa. Based on the same thinking, the trend still holds true for a multicomponent solid solution. In summary, the present study predicts that lattice distortion effect in a solid solution alloy would cause a decrease of melting point or melting range. In addition, negative mixing enthalpy would cause a temperature increase whereas positive mixing enthalpy would cause a temperature decrease.

According to melting temperatures measured in this study, the melting temperature drop, $(T_{m0} - T_{m1})$, is a positive value, which indicates the value of $\Delta H_{strain} + \Delta H_{chem}$ should also be positive according to Eq. (7). In the present study mixing enthalpy is negative for the alloy series as listed in Table 4. As a result, the strain energy would be larger than the absolute value of negative chemical bonding energy difference. This demonstrates that lattice distortion is the primary cause for the decrease in melting temperature in the present alloy series.

3.4.6. Lattice distortion effect on thermal conductivity

The transmission carriers of heat or energy involve electrons and phonons. In pure metals, this conduction was dominated by free electrons near the Fermi surface at all temperatures. In impure metals or in disordered alloys, the electron mean free path is further reduced by collision with solute atoms. So, heat conduction in alloys is affected by solutes and defects within the matrix as well as the interference among the free electrons within the system [34–38].

The thermal conductivity $\kappa(T)$ of a material at temperature T can generally be defined according to the relationship $\kappa(T) = \alpha(T) \cdot \rho(T) \cdot C_p(T)$, where $\alpha(T)$ is thermal diffusivity, $\rho(T)$ is density and $C_p(T)$ is specific heat [36]. In this study, we calculated the specific heat of each as-homogenized alloy using the rule of mixture as follows:

$$C_p = \sum X_i C_p^i \tag{8}$$

where X_i and C_p^i are the molar fraction and specific heat of constituent element i, respectively. The C_p^ivalues of the selected

elements are listed in Table 1. By combining measured α and ρ, and calculated C_p, we can obtain the value of κ. Fig. 11(a) shows drastically drops of κ with an increase in the number of elements and attains the minimum level at NiCoFeCr and NiCoFeCrMn alloy. These trends associated with the number of elements do not vary with testing temperature from 25 °C to 400 °C. We propose that these phenomena could be elucidated in terms of lattice distortion, chemical bonding and magnetic coupling effects which affect free electron density and mean free path. First, consider only atomic size factor, lattice distortion could be directly related to differences in atomic size (δ), and Eq. (9) is commonly used to assess the lattice distortion [19],

$$\delta = 100\sqrt{\sum_{i=1}^{n} c_i(1 - r_i/\bar{r})^2} \tag{9}$$

where $\bar{r} = \sum_{i=1}^{n} c_i r_i$, c_i and r_i are the atomic percentage and atomic radius of the ith element, respectively. With the increased number of elements in the alloys, the degree of lattice distortion becomes increasingly severe as indicated in Fig. 11(b), reinforcing the scattering effect between free electrons and lattice and resulting in the suppression of thermal conduction. Second, when adding foreign elements to an alloy system, the nature of the chemical bonds will be altered due to the excess interaction between unlike atomic pairs. As reflected by Table 4 and Fig. 11(b), the magnitude of mixing enthalpy due to excess chemical bonding of the alloy series increases with the number of elements. Its increase is also expected to reduce thermal conduction since stronger bonding could localize the free electron and in turn limits their heat conduction capability. Third, chemical bonding differences between atomic pairs due to electronic and magnetic interaction connected to the same lattice point are also factors. Jin et al. have demonstrated that mixed ferro/antiferro-magnetic state provides an additional source of disorder scattering in alloys containing a mixture of ferromagnetically coupled (Ni, Co, Fe) and antiferromagnetically coupled (Cr and Mn) elements [39]. This magnetic coupling effect would further contribute to the low thermal conductivity of NiCoFeCr and NiCoFeCrMn.

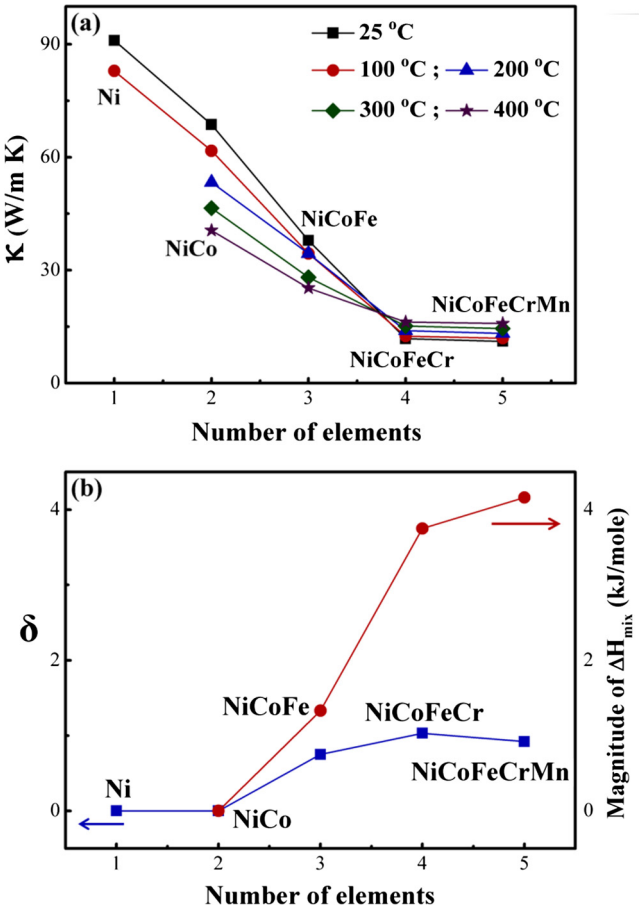

Fig. 11. (a) Thermal conductivities of as-homogenized Ni-Co-Fe-Cr-Mn alloy series. (b) Variations of mixing enthalpy (ΔH_{mix}) magnitude and atomic size difference (δ) with number of elements in as-homogenized Ni-Co-Fe-Cr-Mn alloy series.

As for the similar thermal-conductivity level of NiCoFeCr and NiCoFeCrMn, it could be attributable to their similar δ and mixing enthalpies as shown in Fig. 11 even though the thermal conductivity of Cr and Mn are quite different as seen in Table 1. However, it is noted that only these atomic size and bonding effects could not explain the significant decrease of thermal conductivity from Ni to NiCo since atomic size difference and mixing enthalpy due to excess chemical bonding of NiCo is too small. Moreover, no antiferromagnetically coupled elements lead to mixed ferro/antiferromagnetic state in NiCo alloys, which cause decrease in thermal conductivity [39]. It is apparent that, as discussed in section 5.3, in addition to atomic size difference and bonding difference, crystal structure difference also increases lattice distortion. In fact, as verified by EXAFS analyses, NiCo has remarkable lattice distortion and was used to account for its significant diffuse scattering of X-ray. Similarly, we propose that such lattice distortion would also cause significant scattering of free electrons and thus explain the significant decrease of thermal conductivity. Although it is believed that there is an interesting analogue between X-ray scattering and free electron scattering with lattice distortion, the actual correlation still requires further clarification in the future.

It is interesting to compare the thermal conductivities of NiFe which is also LECCS FCC alloy from literature [39,40] for further discussion with the present data of experimental alloy series. The NiFe alloy has a thermal conductivity of 28.0 W/m K and significantly smaller than that, 70 W/m K, of NiCo alloy and slightly smaller than that, 42 W/m K of NiCoFe alloy. All these have no mixed ferro/antiferro-magnetic state to provide an additional source of disorder scattering. Thus, larger atomic size difference between Ni and Fe (1.25 and 1.27 Å, respectively), crystal structure difference (FCC and BCC, respectively), and larger bonding strength difference (ΔH_{mix} of Ni-Co and Ni-Fe: 0 and −2 kJ/mol, respectively) could be regarded as the main factors to cause NiFe alloy to have thermal conductivity smaller than NiCo and NiCoFe.

Fig. 12 shows the variation of thermal diffusivity (T_D) with temperature for Al-Cr-Fe-Mn-Ni-Mo alloys previously reported [41] and the present as-homo Ni-Co-Fe-Cr-Mn alloy series. It is noted that thermal diffusivities of pure Al, NiCo (LECSS) and NiCoFe (MECSS) alloys decrease, but that of Al-Cr-Fe-Mn-Ni-Mo (MECSS), NiCoFeCr (MECSS or HECSS) and NiCoFeCrMn (HECSS) alloys increase with an increase in temperature. The drop in thermal conductivity and thermal diffusivity with an increase in temperature for pure metals and conventional alloys, as seen in the cases of pure Al, NiCo and NiCoFe alloys, are well-known and can be mainly attributed to an enhanced scattering effect caused by increased electron-phonon interactions. However, the mechanism involved in heat conduction in NiCoFeCr and NiCoFeCrMn alloys differs from that in conventional alloys. Chou et al. also reported similar phenomena and explained why all $Al_xCoCrFeNi$ high-entropy alloys ($0 \leq x \leq 2$) have increased thermal conductivity with temperature [42]. They attributed this increase to the increased lattice spacing due to lattice expansion and thus increased mean free path of conducting electrons. As severe lattice distortion effect largely reduces thermal conductivity by severe electron scattering and results in its low sensitivity to increased thermal vibration with increasing temperature, the greater thermal expansion of these alloys at

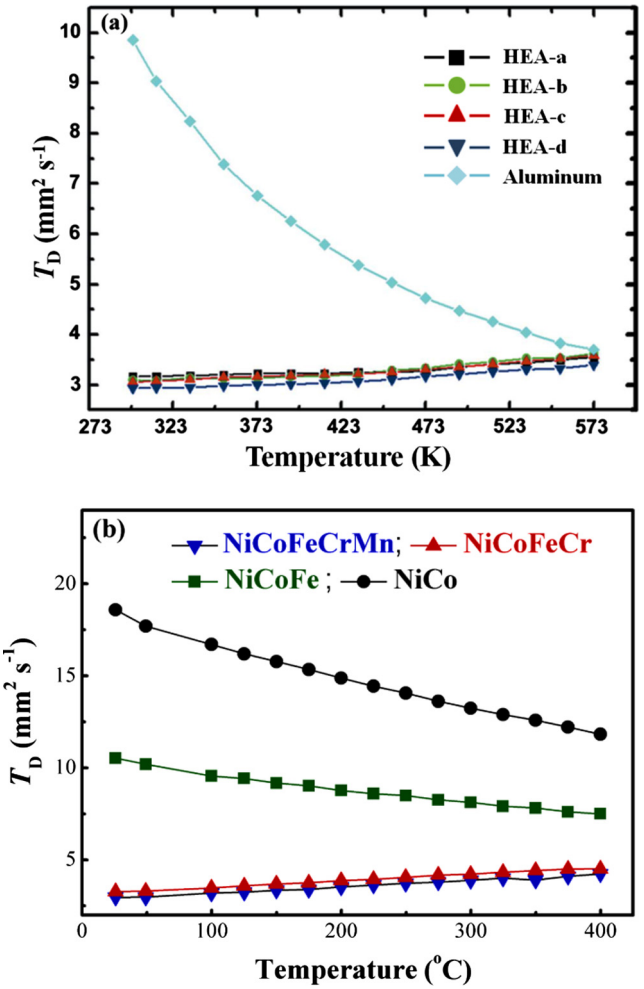

Fig. 12. Variations in thermal diffusivity with temperature for (a) Al-Cr-Fe-Mn-Ni-Mo [41] and (b) as-homogenized Ni-Co-Fe-Cr-Mn alloy series.

higher temperature means that the increased mean free path of electrons and thus thermal conductivity increase with temperature [42]. This mechanism was also verified by Lu et al. [41]. They found that T_D in high-entropy Al-Cr-Fe-Mn-Ni-Mo systems increases at elevated temperatures and explained this phenomenon with the lengthening of the mean free path upon thermal expansion, which scaled with lattice dilation over a wide range of temperatures. However, more quantitative theory is still required for this interesting mechanism.

3.4.7. Summary of physical property evolution and mechanisms

The investigation on atomic configuration, lattice distortion, diffuse scattering, melting point, and thermal conductivity of the alloy series of Ni-Co-Fe-Cr-Mn: Ni (pure metal), NiCo (LECSS), NiCoFe (MECSS), NiCoFeCr (MECSS or HECSS), and NiCoFeCrMn (HECSS) leads to several important points:

1. Lattice constants positively deviate from that predicted by the rule of mixture. The deviation increases with increased number of elements and attains 1.4% for NiCoFeCrMn alloy, which strongly suggests that lattice distortion has the effect to expand the lattice.
2. Examination of NiCoFeCrMn by EXAFS technique reveals that atomic size difference among composing elements is not the only one factor bringing about lattice distortion, the crystal structure difference and chemical bonding difference are important factors as well.
3. X-ray peak intensity significantly decreases from Ni to NiCoFeCrMn at 25 °C. This phenomenon can be explained by increased diffuse scattering due to increased lattice distortion. The diffused scattering due to lattice distortion far exceeds that due to thermal vibration up to 800 °C.
4. The negative deviation of average melting temperature from rule-of-mixture melting point is larger with an increase in the number of composing elements. Lattice distortion effect in the present solid solution alloys is the primary cause to explain this deviation.
5. Thermal conductivity drops fast with an increase in the number of composing elements and attains the minimum level at NiCoFeCr and NiCoFeCrMn alloys. Increased lattice distortion is the main cause. This again confirms that crystal structure difference between Ni and Co causes significant lattice distortion of NiCo. However, magnetic interactions are further noticed in the NiCoFeCr and NiCoFeCrMn alloys. The mixed ferro/antiferromagnetic states in these two alloys further suppress the thermal conductivity.
6. Thermal diffusivities of NiCo and NiCoFe alloys decrease, but that of NiCoFeCr and NiCoFeCrMn alloys increase with an increase in temperature. For NiCoFeCr and NiCoFeCrMn alloys with larger lattice distortion, the increased thermal conductivity by lattice expansion due to thermal vibration overwhelms the decreased thermal conductivity by lattice distortion caused by thermal vibration. As a result, their overall thermal conductivity increases with increasing temperature.

3.5. Cocktail effect in concentrated solid solutions

High mixing entropy could enhance the formation of multi-element solid solutions. By thermodynamics equilibrium, HEAs might have simple phase, two phases, three phases or more to attain the lowest free energy depending on the composition and temperature. Processing could also change the phases by kinetics reason. Nevertheless, the whole properties are from the overall contribution of the constituent phases by the effects of grain morphology, grain size distribution, grain and phase boundaries, and the properties of each phase. Each phase is most frequently a CSS which can be regarded as atomic-scale composite. Their composite properties not only come from the basic properties of elements by the mixture rule but also from the mutual interactions among all the elements and from the severe lattice distortion. Therefore, cocktail effect is the overall effect from composition, crystal structure, lattice distortion, and microstructure. For example, lightweight alloys should use light metal elements [43]; High melting point alloys need refractory elements [44–46]; and oxidization resistant alloys require the addition of Al, Cr, or Si [47,48]. Nonetheless, mutual interactions, difference of atomic size and crystal structure, and kinetics must be considered for the pros and cons on properties [49–52]. Even so, we still have a high degree of freedom and flexibility to design the composition and process to fulfill the predetermined requirements.

4. Conclusions

High-entropy concentrated solid solutions (HECSS), medium-entropy ones (MECSS) and low-entropy ones (LECSS) could be defined based on configurational entropy for concentrated solid solution, having the physical meaning of entropy effect. Physical metallurgy principles might be different from that of current physical metallurgy which mainly bases on dilute solid solution (DSS). Four core effects become more and more pronounced in higher-order solid solution. In addition to the core effects on mechanical properties which were briefly explained, the core effects especially

lattice distortion effect on physical properties of a series of Ni-Co-Fe-Cr-Mn alloys: Ni (pure metal), NiCo (LECSS), NiCoFe (MECSS), NiCoFeCr (MECSS or HECSS), and CoCrFeMnNi (HECSS) are presented with the property evolution. All these demonstrate that four core effects are helpful for the understanding of concentrated solid solutions, which is the base for understanding low entropy to high entropy multi-phase alloys.

Acknowledgement

The authors gratefully acknowledge the financial support for this research from the Ministry of Science and Technology of Taiwan under Grant No. MOST 102-2221-E-007-047-MY3.

References

[1] R.W. Cahn, P. Haasen, Physical Metallurgy, third ed., North-Holland, Amsterdam, 1983, pp. 1–35.
[2] R.E. Reed-Hill, R. Abbaschian, Physical Metallurgy Principles, third ed., PWS Publishing Company, Boston, 1994, pp. xiii–xv.
[3] J.W. Yeh, S.K. Chen, S.J. Lin, J.Y. Gan, T.S. Chin, T.T. Shun, C.H. Tsau, S.Y. Chang, Nanostructured high-entropy alloys with multiple principal elements: novel alloy design concepts and outcomes, Adv. Eng. Mater. 6 (2004) 299–303.
[4] J.W. Yeh, Recent progress in high-entropy alloys, Ann. Chim. – Sci. Mater. 31 (2006) 633–648.
[5] J.W. Yeh, Alloy design strategies and future trends in high-entropy alloys, JOM 65 (2013) 1759–1771.
[6] Y. Zhang, T.T. Zuo, Z. Tang, M.C. Gao, K.A. Dahmen, P.K. Liaw, Z.P. Lu, Microstructures and properties of high-entropy alloys, Prog. Mater. Sci. 61 (2014) 1–93.
[7] D.B. Miracle, O.N. Senkov, A critical review of high entropy alloys and related concepts, Acta Mater. 122 (2017) 448–511.
[8] L.J. Santodonato, Y. Zhang, M. Feygenson, C.M. Parish, M.C. Gao, R.J.K. Weber, J. C. Neuefeind, Z. Tang, P.K. Liaw, Deviation from high-entropy configurations in the atomic distributions of a multi-principal-element alloy, Nat. Commun. 6 (2015) 5964.
[9] J.W. Yeh, Physical metallurgy of high-entropy alloys, JOM 67 (2015) 2254–2261.
[10] M.C. Gao, J.W. Yeh, P.K. Liaw, Y. Zhang, High-Entropy Alloys: Fundamentals and Applications, Springer, Switzerland, 2015, pp. 51–114.
[11] K.Y. Tsai, M.H. Tsai, J.W. Yeh, Sluggish diffusion in Co-Cr-Fe-Mn-Ni high-entropy alloys, Acta Mater. 61 (2013) 4887–4897.
[12] C.S. Barrett, T.B. Massalski, Structure of Metals, third ed., McGraw-Hill, New York, 1966.
[13] D.R. Lide, CRC Handbook of Chemistry and Physics, 72nd ed., CRC Press, Boca Raton, 1991.
[14] C. Kittel, Introduction to Solid State Physics, 8th ed., John Wiley & Sons, New York, 2004.
[15] B.D. Cullity, S.R. Stock, Elements of X-ray Diffraction, third ed., Prentice-Hall, New Jersey, 2001.
[16] A.R. Denton, N.W. Ashcroft, Vegard law, Phys. Rev. A 43 (1991) 3161–3164.
[17] G. Bozzolo, J. Ferrante, J.R. Smith, Method for calculating alloy energetics, Phys. Rev. B 45 (1992) 493–496.
[18] X. Yang, Y. Zhang, Prediction of high-entropy stabilized solid-solution in multi-component alloys, Mater. Chem. Phys. 132 (2012) 233–238.
[19] S. Guo, C.T. Liu, Phase stability in high entropy alloys: Formation of solid solution phase or amorphous phase, Prog. Nat. Sci. 21 (2011) 433–446.
[20] V.A. Lubarda, On the effective lattice parameter of binary alloys, Mech. Mater. 35 (2003) 53–68.
[21] I. Toda-Caraballo, P.E.J. Rivera-Diaz-del-Castillo, Modelling solid solution hardening in high entropy alloys, Acta Mater. 85 (2015) 14–23.
[22] J.J. Rehr, R.C. Albers, Theoretical approaches to x-ray absorption fine structure, Rev. Mod. Phys. 72 (2000) 621–654.
[23] F.W. Lytle, The EXAFS family tree: a personal history of the development of extended X-ray absorption fine structure, J. Synchrotron. Radiat. 6 (1999) 123–134.
[24] A. Filipponi, A. DiCicco, X-ray-absorption spectroscopy and n-body distribution functions in condensed matter II. Data analysis and applications, Phys. Rev. B 52 (1995) 15135–15149.
[25] V.G. Harris, K.M. Kemner, B.N. Das, N.C. Koon, A.E. Ehrlich, J.P. Kirkland, J.C. Woicik, P. Crespo, A. Hernando, A.G. Escorial, Near-neighbor mixing and bond dilation in mechanically alloyed Cu-Fe, Phys. Rev. B 54 (1996) 6929–6940.
[26] G. Renaud, N. Motta, F. Lancon, M. Belakhovsky, Topological short range disorder in $Au_{1-x}Ni_x$ solid solutions – an extended X-ray absorption fine structure spectroscopy and computer simulation study, Phys. Rev. B 38 (1988) 5944–5964.
[27] J.M.C. Thornton, P. Unsworth, M.A. Newell, P. Weightman, C. Jones, R. Bilsborrow, D. Norman, Local lattice distortion in ordered and disordered Cu_3Pd alloys, Europhys. Lett. 26 (1994) 259–264.
[28] C.W. Tucker, P. Senio, X-ray scattering effects due to localized static lattice defects, Phys. Rev. 99 (1955) 1777–1781.
[29] B. Borie, X-ray diffraction effects of atomic size in alloys, Acta Crystallogr. 10 (1957) 89–96.
[30] J.W. Yeh, S.Y. Chang, Y.D. Hong, S.K. Chen, S.J. Lin, Anomalous decrease in X-ray diffraction intensities of Cu-Ni-Al-Co-Cr-Fe-Si alloy systems with multi-principal elements, Mater. Chem. Phys. 103 (2007) 41–46.
[31] W.A. Oates, Configurational entropies of mixing in solid alloys, J. Phase Equilib. Diffus. 28 (2007) 79–89.
[32] R.A. Swalin, Thermodynamics of Solid, second ed., John Wiley & Sons, New York, 1972.
[33] D.A. Porter, K.E. Easterling, Phase Transformation in Metals and Alloys, second ed., Nelson Thornes, Cheltenham, 1992.
[34] J.E. Parrott, A.D. Stuckes, Thermal Conductivity of Solids, Pion, London, 1975.
[35] P.G. Klemens, Thermal resistance due to point defects at high temperatures, Phys. Rev. 119 (1960) 507–509.
[36] S.C. Jain, T.C. Goel, V. Narayan, Thermal conductivity of metals at high temperatures by the Jain and Krishnan method III. Platinum, J. Phys. D – Appl. Phys. (1969) 109–113.
[37] R.J.M. Vanvucht, H. Vankempen, P. Wyder, Simple transport properties of simple metals – classical theories and modern experiments, Rep. Prog. Phys. 48 (1985) 853–905.
[38] R. Venkatasubramanian, Lattice thermal conductivity reduction and phonon localizationlike behavior in superlattice structures, Phys. Rev. B 61 (2000) 3091–3097.
[39] K. Jin, B.C. Sales, G.M. Stocks, G.D. Samolyuk, M. Daene, W.J. Weber, Y. Zhang, H. Bei, Tailoring the physical properties of Ni-based single-phase equiatomic alloys by modifying the chemical complexity, Sci. Rep. 6 (2016) 20159.
[40] A.J. Zaddach, C. Niu, C.C. Koch, D.L. Irving, Mechanical properties and stacking fault energies of NiFeCrCoMn high-entropy alloy, JOM 65 (2013) 1780–1789.
[41] C.L. Lu, S.Y. Lu, J.W. Yeh, W.K. Hsu, Thermal expansion and enhanced heat transfer in high-entropy alloys, J. Appl. Crystallogr. 46 (2013) 736–739.
[42] H.P. Chou, Y.S. Chang, S.K. Chen, J.W. Yeh, Microstructure, thermophysical and electrical properties in $Al_xCoCrFeNi$ ($0 \leq x \leq 2$) high-entropy alloys, Mater. Sci. Eng. B – Adv. Funct. Solid-State Mater. 163 (2009) 184–189.
[43] K.M. Youssef, A.J. Zaddach, C.N. Niu, D.L. Irving, C.C. Koch, A Novel low-density, high-hardness, high-entropy alloy with close-packed single-phase nanocrystalline structures, Mater. Res. Lett. 3 (2015) 95–99.
[44] O.N. Senkov, G.B. Wilks, D.B. Miracle, C.P. Chuang, P.K. Liaw, Refractory high-entropy alloys, Intermetallics 18 (2010) 1758–1765.
[45] O.N. Senkov, S.V. Senkova, C. Woodward, D.B. Miracle, Low-density, refractory multi-principal element alloys of the Cr-Nb-Ti-V-Zr system: microstructure and phase analysis, Acta Mater. 61 (2013) 1545–1557.
[46] C.C. Juan, M.H. Tsai, C.W. Tsai, C.M. Lin, W.R. Wang, C.C. Yang, S.K. Chen, S.J. Lin, J.W. Yeh, Enhanced mechanical properties of HfMoTaTiZr and HfMoNbTaTiZr refractory high-entropy alloys, Intermetallics 62 (2015) 76–83.
[47] W.J. Shen, M.H. Tsai, K.Y. Tsai, C.C. Juan, C.W. Tsai, J.W. Yeh, Y.S. Chang, Superior oxidation resistance of $(Al_{0.34}Cr_{0.22}Nb_{0.11}Si_{0.11}Ti_{0.22})_{50}N_{50}$ high-entropy nitride, J. Electrochem. Soc. 160 (2013) C531–C535.
[48] C.M. Liu, H.M. Wang, S.Q. Zhang, H.B. Tang, A.L. Zhang, Microstructure and oxidation behavior of new refractory high entropy alloys, J. Alloys Compd. 583 (2014) 162–169.
[49] C.W. Tsai, S.W. Lai, K.H. Cheng, M.H. Tsai, A. Davison, C.H. Tsau, J.W. Yeh, Strong amorphization of high-entropy AlBCrSiTi nitride film, Thin Solid Films 520 (2012) 2613–2618.
[50] Y. Dong, K.Y. Zhou, Y. Lu, X.X. Gao, T.M. Wang, T.J. Li, Effect of vanadium addition on the microstructure and properties of AlCoCrFeNi high entropy alloy, Mater. Des. 57 (2014) 67–72.
[51] C.M. Lin, C.C. Juan, C.H. Chang, C.W. Tsai, J.W. Yeh, Effect of Al addition on mechanical properties and microstructure of refractory $Al_xHfNbTaTiZr$ alloys, J. Alloys Compd. 624 (2015) 100–107.
[52] C.Y. Cheng, J.W. Yeh, High thermal stability of the amorphous structure of $Ge_xNbTaTiZr$ (x = 0.5, 1) high-entropy alloys, Mater. Lett. 181 (2016) 223–226.